Stem Cell Reports
Article

ISSCR

OPEN ACCESS

Integrin β1 activity controls colony morphology during human pluripotent stem cell state transitions

Maria E. Taskinen,[1] Nicolas Pasquier,[1,7,8] Aki Stubb,[1,8] Shreya Joshi,[1] Megan R. Chastney,[1] Paula Rasila,[1] Sonja Vahlman,[1] Joonas Sokka,[2] Tapio Lönnberg,[1,3] Lea Mikkola,[1,3] Ras Trokovic,[2] and Johanna Ivaska[1,3,4,5,6,9,*]

[1]Turku Bioscience Centre, University of Turku and Åbo Akademi University, FI-20520 Turku, Finland
[2]Research Programs Unit, Stem Cells and Metabolism and Biomedicum Stem Cell Centre, Faculty of Medicine, University of Helsinki, FI-00014 Helsinki, Finland
[3]InFLAMES Research Flagship Center, University of Turku, FI-20520 Turku, Finland
[4]Department of Life Technologies, University of Turku, FI-20520 Turku, Finland
[5]Western Finnish Cancer Center (FICAN West), University of Turku, FI-20520 Turku, Finland
[6]Foundation for the Finnish Cancer Institute, Tukholmankatu 8, FI-00014 Helsinki, Finland
[7]INSERM U-1279, Gustave Roussy, F-94805 Villejuif, France
[8]These authors are equal contribution
[9]Lead contact
*Correspondence: johanna.ivaska@utu.fi
https://doi.org/10.1016/j.stemcr.2025.102538

SUMMARY

Integrin β1-mediated adhesion is dispensable in early mouse embryogenesis (pre-implantation) but indispensable post-implantation, suggesting distinct roles for β1-integrin-mediated adhesions in the naive (pre-implantation) versus primed (post-implantation) pluripotent stem cells (PSCs). We investigated the role of integrin β1 in regulating naive-like and primed human induced PSC (hiPSC) states. We find that integrin β1 is active in both *in vitro*. In primed hiPSCs, integrin β1 inhibition induces naive-like colony features, reduces actomyosin contraction and extracellular signal-regulated kinase (ERK) activity, and alters gene expression, indicative of more naive-like features. These resemble the dramatic reorganization of the colony morphology, actin cytoskeleton, and adhesions upon chemical reversion from primed to naive states of pluripotency. Importantly, functional and single-cell transcriptomics analyses demonstrate that integrin β1 inhibition attenuates colony morphology transitions in cells exiting naive pluripotency. These data reveal unprecedented integrin-dependent regulation of PSC states and demonstrate how integrin inhibitors may help to fine-tune hiPSC function and properties *in vitro*.

INTRODUCTION

Integrins are heterodimeric cell-surface receptors that mediate adhesion to the extracellular matrix (ECM) and are connected to the intracellular actin cytoskeleton (Brakebusch and Fässler, 2003; Campbell and Humphries, 2011; Hynes, 2002). Integrin β1 is essential for the survival and development of mouse embryos. Mouse embryos lacking integrin β1 develop normally until the pre-implantation stage but degenerate at implantation (Fässler et al., 1995; Stephens et al., 1995), implying distinct roles for β1-integrins pre- and post-implantation. However, the functional role of integrin signaling during the pre- to post-implantation transition remains poorly understood. More recently, integrin β1 has been shown to regulate the actomyosin organization in mouse embryos upon implantation (Molè et al., 2021) and mediate proper organization of the epiblast and primitive endoderm in late mouse blastocysts (Kim et al., 2022a). However, integrin β1 regulation and role in controlling actomyosin contractility in human embryonic development remain elusive.

Human induced pluripotent stem cells (hiPSCs) are reprogrammed from human somatic cells and closely resemble embryonic stem cells (ESCs) with their epithelial morphology, gene expression, and function (Takahashi and Yamanaka, 2006; Takahashi et al., 2007). Since pluripotent stem cells (PSCs) are able to self-renew and differentiate into nearly any adult human cell type, they are powerful tools in disease modeling and treatment (Pera and Rossant, 2021). Naive and primed states of pluripotency are well established in mice, where naive PSCs resemble pre-implantation and primed post-implantation epiblast cells (Nichols and Smith, 2009). For human cells, *in vitro* cultured hiPSCs are considered to be in a primed state. They have epithelial-like features and grow in tightly packed colonies delimited by integrin adhesion-dependent cornerstone adhesions connected to an actin "fence" structure (Närvä et al., 2017; Stubb et al., 2019). The position of hiPSCs in the colony, with respect to the edge, correlates with different aspects of cell polarity (Kim et al., 2022b). Thus, integrin-mediated focal adhesions and the ECM composition are key regulators of primed hiPSCs maintenance *in vitro*. Human naive-like cells can be generated from hiPSCs using various methods (Bredenkamp et al., 2019; Collier et al., 2022; Hassani et al., 2019; Taei et al., 2020; Theunissen et al., 2014). The naive-like cells differ from the primed cells in their gene expression patterns and signaling pathways (Lynch et al., 2020; Martinez-Val

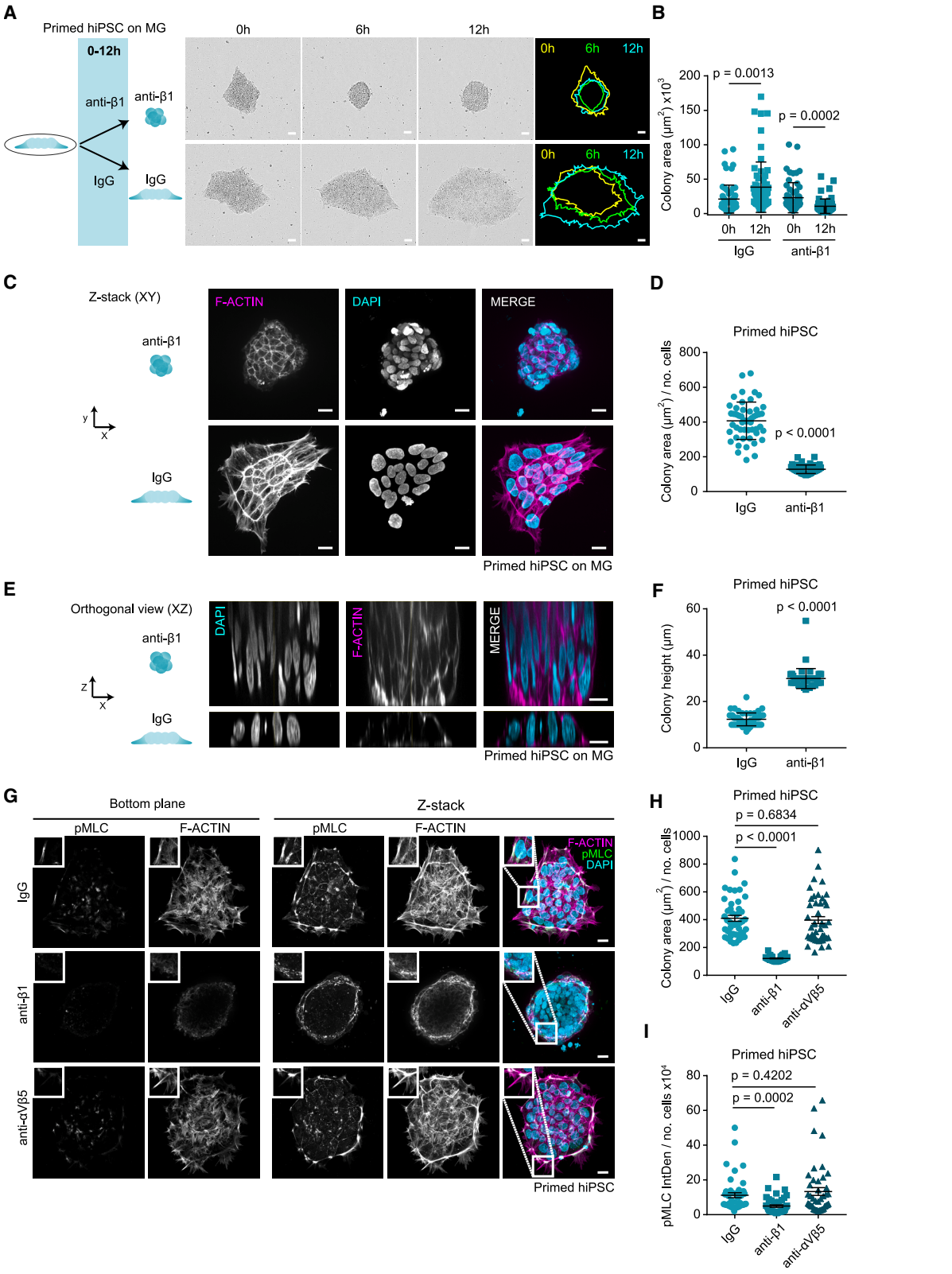

(legend on next page)

et al., 2021; Nichols et al., 2009; Sim et al., 2017; Takashima et al., 2014; Weinberger et al., 2016) and adopt a dome-like colony morphology. This suggests that integrin-mediated ECM interactions in human naive-like PSCs are distinct from the previously described cornerstone focal adhesions in primed hiPSCs (Närvä et al., 2017; Stubb et al., 2019) and would have biologically distinct functions *in vitro*. This, however, has not been investigated in detail. Furthermore, during development, naive PSCs must transition to a state of primed pluripotency (a process called capacitation) to facilitate the formation of the germ layers (Rostovskaya et al., 2019). The role of cell-ECM interactions in this crucial step remains unknown. Naive hiPSCs open a window to early human development and disease modeling, thus further understanding their regulation by adhesions *in vitro* is needed.

Here, we demonstrate that integrin β1 is active in naive and primed hiPSCs when cultured *in vitro* on commonly used ECMs, Matrigel, vitronectin, and laminin-521. Inhibition of integrin β1 induces naive-like features in primed hiPSCs, including dome-like colony morphology, naive-like gene expression patterns, inhibition of extracellular signal-regulated kinase (ERK) activity, and reduced actomyosin contraction. Additionally, integrin inhibition impairs exit from pluripotency in naive cell capacitation assays.

RESULTS

Inhibition of integrin β1 alters colony morphology and actomyosin contractility in primed hiPSCs

We have shown, using super-resolution interferometric photoactivation localization microscopy (iPALM), that primed hiPSC colonies are delimited by large integrin β1-positive cornerstone focal adhesions and sharp actin-fenced edges on different ECM (Stubb et al., 2019). To investigate the functional relevance of integrin β1 activity for maintaining primed hiPSC colony morphology, we used a function-blocking integrin antibody (MAb13; anti-β1). Within 12 h of integrin inhibition, there was a notable rearrangement of the flat two-dimensional sharp-edged primed hiPSC colonies into tightly packed, more dome-shaped structures, resembling to some degree the morphology of naive hiPSC colonies (Figures 1A–1F, Videos S1 and S2). Integrin β1 inhibition significantly decreased the colony area (Figures 1A and 1B), induced tighter cell clustering (Figures 1C and 1D), increased the colony height (Figures 1E and 1F), increased the total cell number (Figure S1A), and triggered reorganization of actin with loss of extended stress fibers. To confirm our findings, we tested another integrin β1 function-blocking antibody, AIIB2, which triggered a similar morphological change observed with MAb13 (Figure S1B). These data suggest that integrin β1 is required to mediate primed hiPSC colony spreading. On the other hand, the protein levels of OCT4, a transcription factor essential in the maintenance of primed pluripotency (Weinberger et al., 2016), were not significantly altered (Figures S1C and S1D), indicating that integrin inhibition alone does not alter pluripotency regulator expression under these culture conditions.

Integrin αVβ5 is also highly expressed specifically at the edges of the primed hiPSC integrin β1-positive cornerstone focal adhesions (Stubb et al., 2019). To determine the relative contribution of these adhesion receptors to primed hiPSCs' colony morphology and actin organization, we incubated the cells with immunoglobulin G (IgG) (control), anti-β1, or anti-αVβ5 antibodies. Inhibition of integrin β1 or αVβ5 had no significant effect on OCT4 protein levels after 24 h (Figures S1E and S1F). However, immunofluorescence staining of F-actin and phosphorylated myosin light chain (pMLC) revealed significant cytoskeletal differences. Integrin β1 inhibition reduced colony area, induced tighter cell clustering, and increased the total cell number, whereas αVβ5 inhibition had no significant effect (Figures 1G–1I and S1G). Even though the more tightly packed organization, induced by integrin β1 inhibition,

Figure 1. Integrin β1 inhibition alters primed hiPSC colony morphology

(A and B) Representative bright-field images (A) and colony area quantification (B) of primed hiPSCs on Matrigel (MG) after 0, 6, and 12 h IgG or MAb13 anti-integrin β1 (anti-β1) treatment. Scale bar, 50 μm. (3 independent experiments, unpaired t test with Welch's correction, mean ± SD).

(C and D) z stacks (C; maximum intensity projections) of representative SiR-actin (F-actin) and DAPI staining in primed hiPSCs on Matrigel after 12 h IgG or anti-β1 treatment and quantification (D) of cell colony area (based on F-actin staining) normalized to cell number (3 independent experiments, 45–51 cell colonies in total, unpaired t test with Welch's correction, mean ± SD). Scale bar, 20 μm.

(E and F) Orthogonal view (E; z axis) of representative SiR-actin (F-actin) and DAPI staining in primed hiPSCs on Matrigel after 12 h IgG or anti-β1 treatment and quantification of colony height (F; 3 independent experiments, 45–51 cell colonies in total, unpaired t test with Welch's correction, mean ± SD). The microscope's working distance limited imaging of the top of the highest colonies. Scale bar, 20 μm.

(G) Representative pMLC, SiR-actin (F-actin), and DAPI staining of primed hiPSCs plated on Matrigel and treated with IgG, anti-β1, or anti-αVβ5 (24 h).

(H and I) Quantification of colony area normalized by cell number (H) and pMLC intensity (I). (3 individual experiments, 44–46 cell colonies in total, unpaired t test with Welch's correction, mean ± SEM). See also Figure S1.

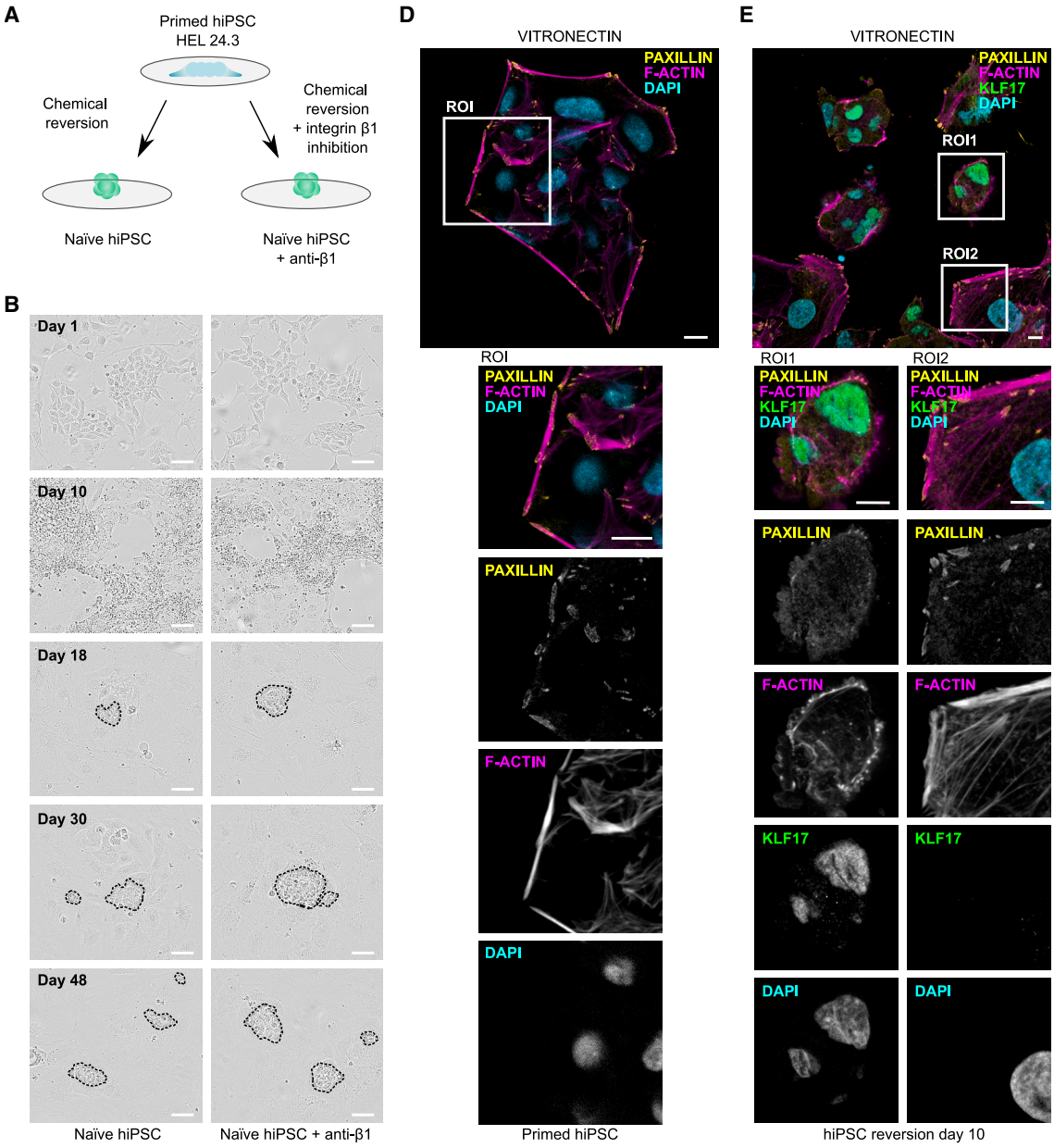

(legend on next page)

would imply higher contractility in the colonies, pMLC levels were, in fact, significantly decreased (Figures 1G–1I). In contrast, αVβ5 inhibition did not influence pMLC levels. These results were validated in another primed hiPSC line (Figures S1H–S1J). The staining pattern of contractile cytoskeletal machinery indicates that the active integrin β1 adhesions link to actin fibers that pull the cells toward ECM, limiting colony height in the primed state of pluripotency.

Focal adhesions are lost in KLF17-expressing cells

As integrin β1 inhibition promoted a naive-like compacted colony morphology in primed hiPSCs, we assessed whether integrin β1 inhibition would facilitate the reversion of hiPSCs into a naive-like state. We reverted primed hiPSCs into a naive-like state (using an established protocol involving epigenetic reversion [Guo et al., 2017]) in the presence or absence of the integrin β1 function-blocking antibody (Figure 2A). Interestingly, integrin β1 inhibition increased hiPSC proliferation during the reversion process (Figures S2A and S2B), while cells in both conditions reached a typical dome-shaped morphology apparent on day 18 (Figure 2B). The mRNA levels of primed markers *ZIC2* and *SFRP2* were decreased, and mRNA levels of naive markers *KLF17* and *TBX3* were induced in both naive hiPSC conditions during the reversion, as expected (Figure 2C; mRNA expression in non-reverted primed hiPSC is included as control for all the time points). There was a slight trend for higher naive marker expression in the integrin β1-inhibited cells compared to the control naive cells (Figure 2C). In particular the expression of KLF17 seemed higher at the late time points. However, these were not statistically significant.

To further investigate the role of integrin β1 in the naive and primed cell states, we monitored cell adhesions on different ECMs. Primed hiPSCs formed large integrin-mediated focal adhesions at the edge of the cell colonies on vitronectin (Figure 2D), as reported earlier (Närvä et al., 2017; Stubb et al., 2019). To study focal adhesions in hiPSCs during chemical reversion to a naive-like state, we plated cells on Matrigel, vitronectin, and laminin-521, ECMs commonly used in hiPSC culture, at day 10 of the reset protocol, and performed immunofluorescence staining of paxillin, a major component of focal adhesions, and Krueppel-like factor 17 (KLF17) (Figures 2E, S2C, and S2D). On the 10th day of the reversion, some of the hiPSCs had started to express KLF17 (Figures S2E and S2F). On all of the ECMs investigated, the KLF17-positive cells lacked the clear focal adhesions and prominent actin stress fibers typically detected in the primed-state cells (Figures 2E, S2C, and S2D). KLF17-positive cell populations had a trend of less coherently oriented actin filaments (Figure S2G) and lower F-actin intensity (Figure S2H) when compared to the KLF17-negative cell populations on Matrigel and vitronectin. One of the key mediators of integrin signaling in focal adhesions is Src kinase. Interestingly, reversion to a naive state resulted in strong downregulation of Src activity (detected by Y416 pSrc specific antibody) (Figure S2I). These data indicate that transition from primed to naive-like state is accompanied by striking alteration of cell-ECM adhesion.

To further compare our naive cells with the primed hiPSCs, we studied KLF17 and NANOG (a pluripotency marker) protein expression by western blotting. We found KLF17 expression solely in the naive hiPSCs, while NANOG expression remained similar in both states (Figure S3A). Furthermore, qPCR data indicate that the primed hiPSCs are negative for the naive markers (*KLF17* and *TBX3*) and positive for primed markers (*ZIC2* and *SFRP2*). In both cases, the relative mRNA expression of these genes is concordant with the cell state (Figure S3B). Immunofluorescence data correlated with these observations, demonstrating nuclear KLF17 signal only in the naive cells on different matrices (Matrigel, vitronectin, and laminin-521) (Figure S3C).

Integrin β1 is highly active in naive and primed hiPSCs when cultured *in vitro*

Earlier studies have demonstrated that integrin β1 signaling is dispensable for the formation and survival of the pre-implantation mouse embryo inner cell mass (ICM) (Molè et al., 2021; Stephens et al., 1995) but vital in the subsequent steps of development. According to a cell-surface proteomics study, naive human pluripotent stem cells (hPSCs), which resemble the pre-implantation ICM, have less integrin β1 on their cell surface compared

Figure 2. Chemical reversion into a naive-like state with integrin β1 inhibition

(A) Illustration of the experimental design.

(B) Representative images of hiPSCs on feeder cells (iMEFs) during chemical reversion. The clearly visible naive-like colonies are marked using dashed lines drawn along the colony edge. Scale bar, 20 μm.

(C) Relative mRNA levels of *KLF17*, *TBX3*, *ZIC2*, and *SFRP2* quantified by qPCR in primed (normal culture conditions) and naive hiPSCs during chemical reversion. Naive markers *KLF17* and *TBX3* were normalized to naive hiPSCs' (dashed line), and primed markers *ZIC2* and *SFRP2* were normalized to primed hiPSCs' mRNA expression levels (dashed line) ($N = 1$).

(D) Representative staining of paxillin, SiR-actin (F-actin), and DAPI in primed hiPSCs plated on vitronectin. Scale bar, 10 μm.

(E) Representative staining of paxillin, KLF17, SiR-actin (F-actin), and DAPI in hiPSCs plated on vitronectin after 10 days of chemical reversion. Scale bar, 10 μm. See also Figure S2.

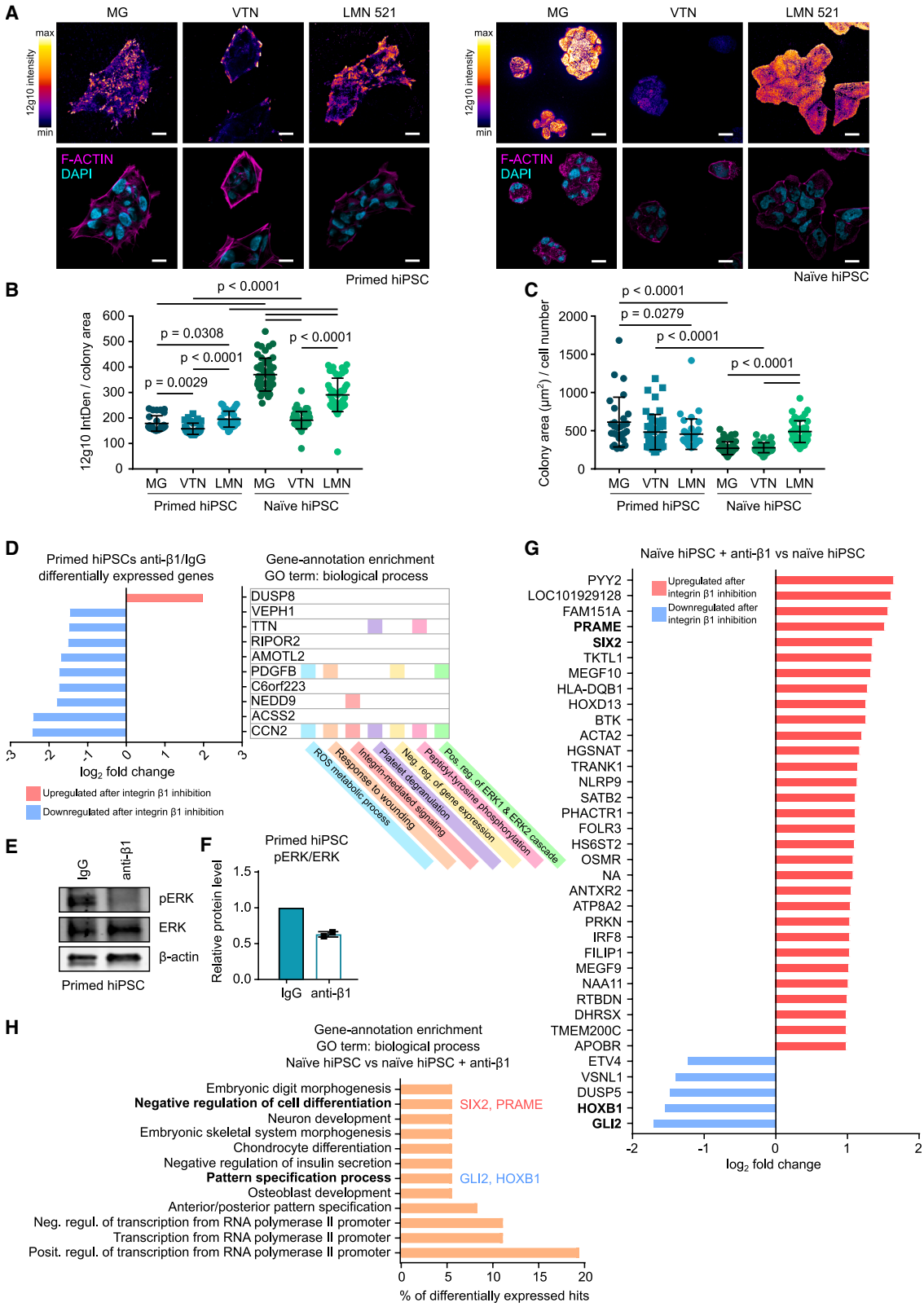

(legend on next page)

to primed hPSCs, which resemble the post-implantation ICM (Wojdyla et al., 2020). These studies, and our data indicative of integrin β1 inhibition inducing a more naive-like colony morphology, prompted us to investigate whether naive hPSC would have less active integrin β1 compared to primed hPSCs. We performed immunofluorescence staining of integrin β1 with an antibody specific for the active ligand-engaged conformation of the receptor (12G10; Byron et al., 2009) in cells cultured on Matrigel, vitronectin, or laminin-521 (Figures 3A–3C and S3C). In primed hiPSCs, active integrin β1 intensity was the highest when cells were cultured on Matrigel and laminin-521. On these ECMs, the primed hiPSCs formed focal adhesions mainly at the edge but also in the middle of the colonies (Figures 3A and 3B). When cultured on vitronectin, the total level of active integrin β1 was lower, but the cells formed prominent cornerstone focal adhesions at the colony edge, as reported earlier (Närvä et al., 2017; Stubb et al., 2019).

Surprisingly, we observed significantly higher integrin activity on all matrices in naive hiPSCs when compared to primed hiPSCs plated on the same matrices (Figures 3A–3C). In addition, human embryonic stem cells (hESCs) that were reverted to a naive state using the same protocol also displayed high levels of active integrin β1 (Figure S3D). Despite high integrin activity, discernable focal adhesions were lacking in naive hiPSCs, and active integrins were distributed across the entire colony's cell-ECM interface. The naive hiPSCs were strongly positive for nuclear KLF17 on all matrices, with the primed cells showing only low non-nuclear signal (Figure S3C). However, on laminin-521, the naive hiPSC colonies were less tightly packed than on vitronectin, where the integrin β1 activity was the lowest (Figure 3C). This suggests that high integrin β1 activity is linked to the ECM conditions of the cells impacting the naive-like colony morphology of hiPSCs without inducing immediate transition from the naive state.

Integrin β1 inhibition promotes expression of genes supporting a naive-like state

Intrigued by the differences in integrin β1-mediated cell-ECM adhesion in naive and primed states, we investigated which integrins are expressed in these cells and how integrin β1 activity affects gene expression by performing an unbiased genome-wide transcriptome analysis in primed and naive hiPSCs. The main integrin subunits expressed in both cell types were β1, β5, α5, α6, and αV (Figure S3E). In addition, primed cells expressed α3 and α7 subunits and naive cells showed higher expression of the immune-cell-specific integrins (αLβ2, αMβ2, αEβ2, and αXβ2, which mediate adhesion to other cells). These data indicate that our approach of inhibiting integrin β1 and αVβ5 is sufficient to test the outcome of blocking adhesion of all the ECM-binding integrin heterodimers (α3β1, α5β1, α6β1, α7β1, αVβ1, and αVβ5) in these cells. We did not detect any differences in integrin expression in the integrin antibody-treated cells when compared to the IgG control cells (Figure S3E). However, we found that in primed hiPSCs 10 genes were differentially expressed upon integrin β1 inhibition (at 12 h) (Figures 3D; Table S1; false discovery rate (FDR) < 0.05). Nine of the differentially expressed genes were downregulated (Figure 3D). Two of the downregulated genes, *PDGFB* and *CCN2*, are involved in the positive regulation of ERK signaling according to gene ontology (GO) annotations. In addition, the only upregulated gene, *DUSP8*, is emerging as a negative regulator of ERK signaling (Ding et al., 2019). Interestingly, inhibition of ERK signaling is reported to support a naive-like state in mouse embryos and hPSCs (Nichols et al., 2009; Takashima et al., 2014). Consistent with our transcriptome analysis, phosphorylated ERK (pERK) protein levels were also decreased in primed hiPSCs after integrin inhibition (Figures 3E and 3F), implying that integrin β1 inhibition attenuates ERK activity, in line with a more naive-like phenotype, in primed hiPSCs.

Figure 3. Integrin β1 activity is higher in naive hiPSCs, and integrin β1 inhibition promotes expression of naive-like state supporting genes

(A) Representative staining of active integrin β1 (12G10), Phalloidin-Atto 647N (F-actin), and DAPI on the bottom plane of primed and naive hiPSCs plated on Matrigel (MG), vitronectin (VTN), or laminin-521 (LMN 521) for 48 h. Scale bar, 20 μm.

(B) Quantification of 12G10 intensity normalized to the colony area (3 independent experiments, 28–48 cell colonies in total, unpaired t test with Welch's correction, mean ± SD).

(C) Quantification of cell colony area (based on F-actin staining) normalized to cell number (3 independent experiments, 28–48 cell colonies in total, unpaired t test with Welch's correction, mean ± SD).

(D, G, and H) represent mRNA sequencing data.

(D) Differentially expressed genes (false discovery rate, FDR < 0.05) and gene-annotation analysis of anti-β1- vs. IgG (control)-treated (12 h) primed hiPSCs.

(E and F) Western blot of phosphorylated ERK (pERK), total ERK, and β-actin in IgG- or anti-β1-treated (12 h) primed hiPSCs and quantification of pERK protein levels normalized to total ERK (2 individual experiments).

(G) Differentially expressed genes in naive hiPSCs vs. naive + anti-β1 hiPSCs (FDR < 0.05).

(H) Gene-annotation enrichment analysis of differentially expressed genes from (G). See also Figure S3.

Next, we compared the control (IgG treated) naive and the anti-β1 naive cell populations. 36 genes were differentially expressed, 5 downregulated and 31 upregulated, following continuous integrin β1 inhibition (Figure 3G). Interestingly, actin cytoskeleton-related genes, *PHACTR-1*, *ACTA2*, and *FILIP1*(Allain et al., 2012; Jarray et al., 2011; Nagano et al., 2002; Schildmeyer et al., 2000; Wiezlak et al., 2012), were upregulated in the anti-β1 naive cells, possibly linking to the differences in colony compaction and actin organization between control and anti-β1 naive hiPSCs. Furthermore, many of the differentially expressed genes were associated with embryonic development and cell differentiation processes according to gene-annotation analysis (Figure 3H). Two of the downregulated genes, *HOXB1* and *GLI2*, are associated with the pattern specification process, and, in contrast, two of the upregulated genes, *SIX2* and *PRAME*, are linked to negative regulation of cell differentiation (Figure 3H). These results suggest that continuous integrin β1 inhibition may support maintenance of a naive-like state on the transcriptional level.

Integrin β1 controls colony morphology in naive hiPSCs

Intrigued by the changes in actin cytoskeleton-related genes in anti-β1 naive cells, we next investigated the morphological changes of the naive colonies. For this, we tested the effect of integrin β1 inhibition in the naive hiPSCs, which were reverted in the presence or absence of integrin β1 inhibitory antibody (anti-β1 naive and control naive, respectively). Withdrawal of the anti-β1 antibody from anti-β1-reverted naive cells resulted in marked flattening and loss of naive-like colony morphology compared to the control naive cells cultured in the presence of the control IgG after 48 h (Figures 4A and 4B). Integrin inhibition had no effect on colony size (F-actin staining) in control naive cells whereas colony area was significantly decreased in the anti-β1-treated anti-β1-reverted naive hiPSC colonies (Figures 4C–4E). pMLC levels were not altered upon integrin β1 inhibition in either naive population (Figures 4C, 4D, and 4F), suggesting that the morphological changes are not a consequence of changes in actomyosin contractility. These data imply that cells reverted in the presence of integrin β1 inhibition may have adapted to these conditions and depend on continuous integrin β1 inhibition to maintain their state and colony morphology.

Blocking integrin β1 delays the capacitation process

Integrin β1 is well described for its role in regulating morphogenesis and survival of the embryonic lineage during the transition from pre-implantation to post-implantation (Molè et al., 2021). *ITGB1* expression is also upregulated when cells undergo a formative transition, exiting the naive state and gaining competence for lineage induction through capacitation (Rostovskaya et al., 2019). However, the role of integrin β1 in the capacitation, which enables primed hiPSCs to evolve from naive hiPSCs has not been explored, prompting us to test the impact of integrin β1 inhibition on capacitation. We cultured naive hiPSC for 48 h with or without integrin β1 inhibition before switching the cells to the capacitation medium. Live imaging revealed that colonies in both conditions retained a characteristic dome shape in naive culture conditions (0 h, Figure 5A). However, after 48 h in the capacitation medium, control colonies lost their dome-shaped morphology and spread, while those with integrin β1 inhibition maintained a dome-shaped morphology similar to naive-like hiPSCs. After 120 h, both conditions presented a primed-like morphology with flattened colonies. Next, we assessed the ability of the capacitated cells to renew in naive culture conditions using a colony formation assay. Naive hiPSCs capacitated for 2 or 5 days, with or without integrin β1 inhibition, were tested for their ability to form colonies in primed culture medium (E8) or naive culture conditions (Figure 5B). Control naive hiPSCs capacitated for 120 h showed a significant reduction in colony formation under naive conditions, indicating exit from the naive state (Figure 5C). Notably, cells capacitated in the presence of integrin β1 inhibition retained their ability to form naive-like hiPSC colonies after 48 and 120 h, suggesting that integrin β1 inhibition may delay the exit from the naive state (Figure 5C).

Taken together, these data suggest that blocking integrin β1 delays the morphological progression of the capacitation process, with anti-β1-treated cells retaining a naive-like hiPSC colony morphology compared to untreated cells, indicative of a role for integrin β1 during the formative transition of naive hiPSCs.

Single-cell transcriptional profiling of integrin β1 inhibition during capacitation

To further understand the changes in gene expression caused by capacitation and integrin β1 inhibition, we performed single-cell RNA sequencing (scRNA-seq). We compared cells from 6 different conditions: naive hiPSCs (d0) cultured with or without anti-β1, naive hiPSCs capacitated (2 days; d2 capNaive) with or without anti-β1, and primed hiPSCs cultured with or without anti-β1. Dimensionality reduction of the RNA expression data revealed that integrin β1 inhibition had a strong effect on the cells: naive and capacitated cells cultured without anti-β1 were more distinct, while cell populations treated with anti-β1 were more similar to each other (Figure 5D). Primed hiPSCs did not respond to the anti-β1 treatment, and the populations fully overlapped (Figure 5D). We then used a set of established markers (Sokka et al., 2022; see methods) of naive

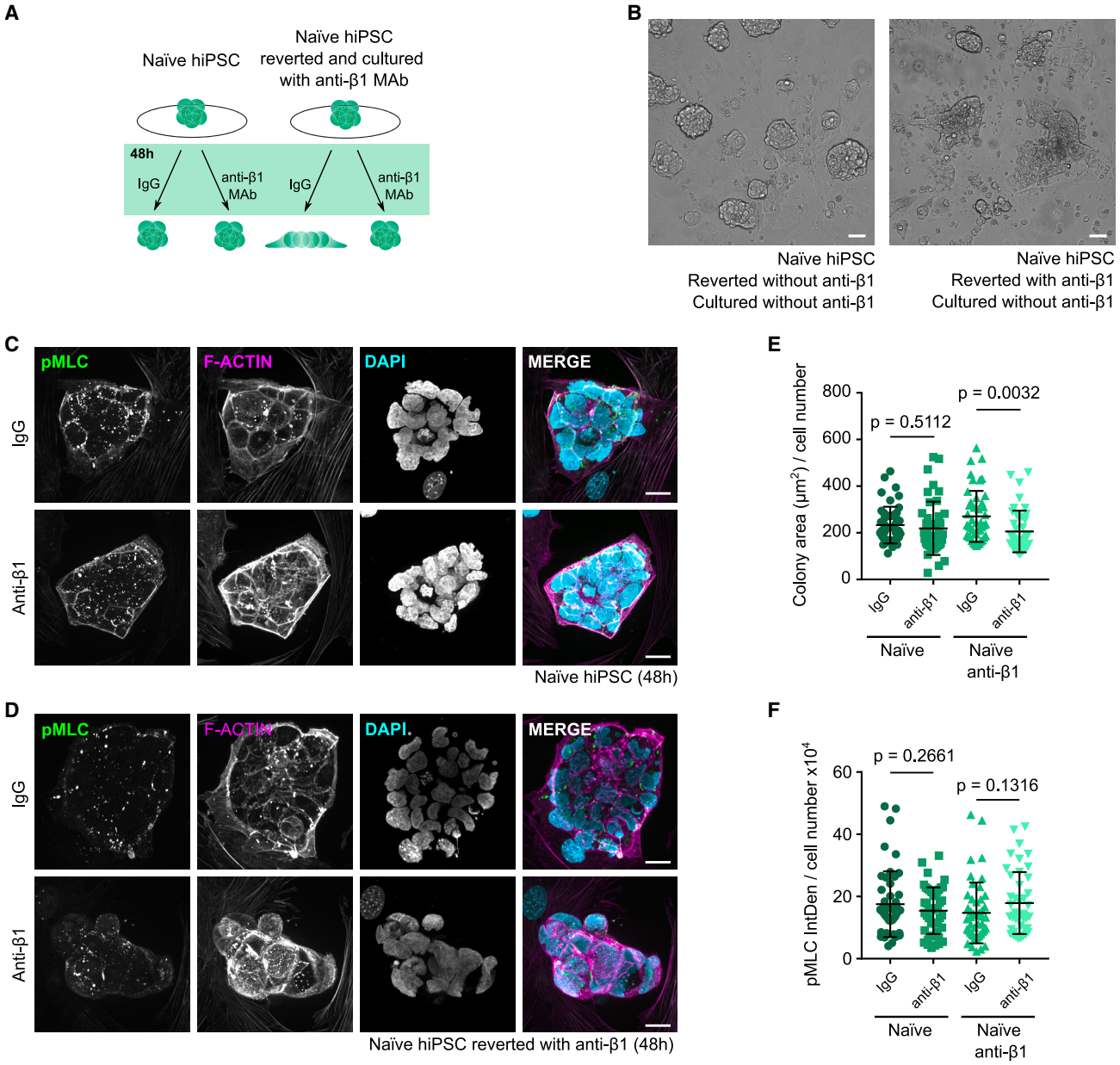

Figure 4. Integrin β1 activity controls colony morphology in naive hiPSCs

(A) Schematic illustration of the experimental design and expected colony morphology (related to B–F).

(B) Representative bright-field images of control or anti-β1-reverted naive hiPSCs cultured on iMEFs without anti-β1 in the culture medium. Scale bar, 50 μm.

(C and D) Representative pMLC, SiR-actin (F-actin), and DAPI staining of control or anti-β1-reverted naive hiPSCs plated on Matrigel and treated with IgG or anti-β1 (48 h).

(E and F) Quantification of colony area normalized by cell number (E) and pMLC intensity (F) (3 individual experiments, 45–51 cell colonies in total, unpaired t test with Welch's correction, mean ± SD).

cell states to calculate module scores, which reflect average expression of the given gene set in the cells. The module scores clearly separated the naive and primed cell states from each other and indicated that integrin β1 inhibition supported a higher module score before and after capacitation (Figures 5E and 5F). To determine the effects of the 48-h capacitation, we ran differential gene expression (DE) analyses between the naive hiPSCs d0 vs. d2 and

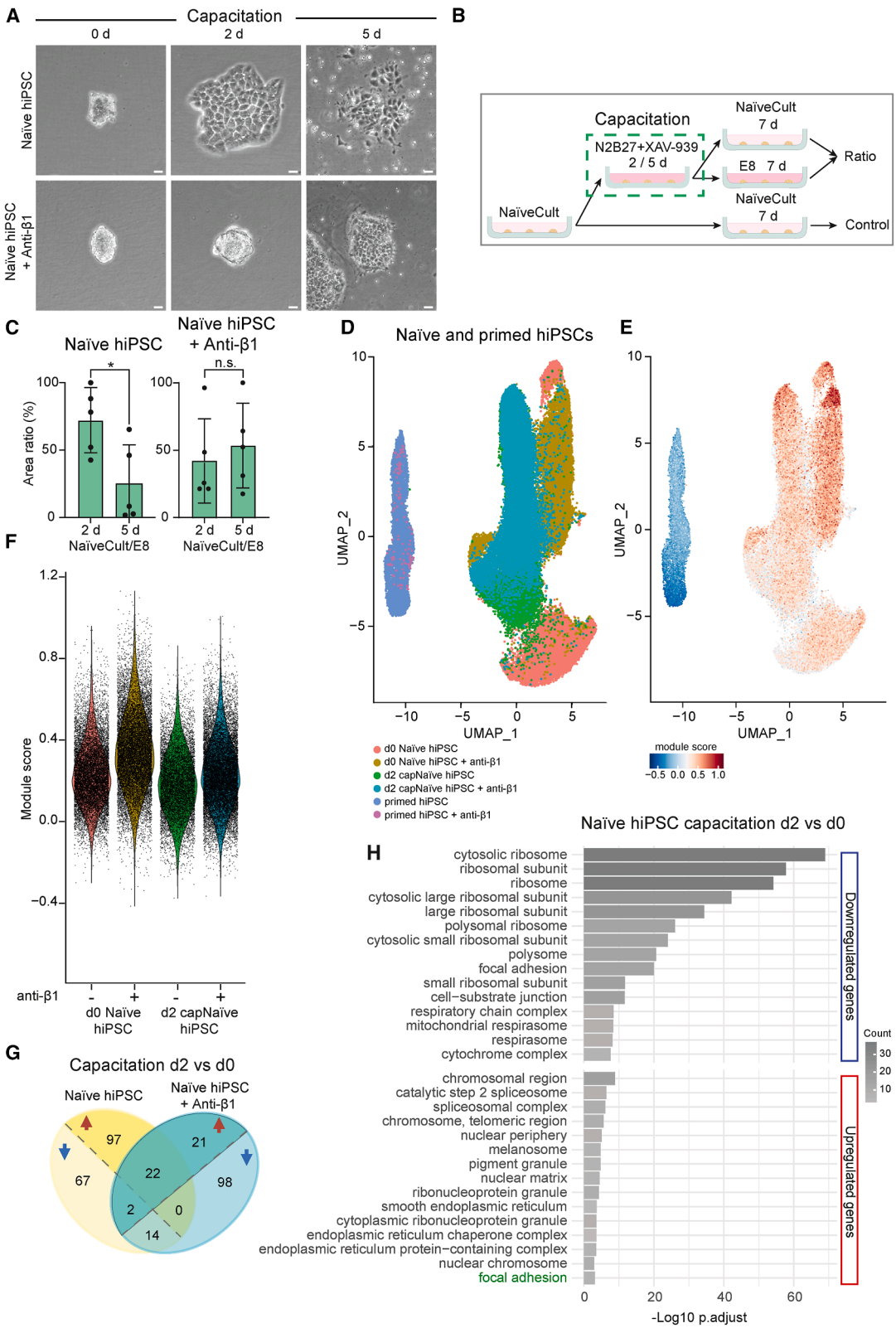

(legend on next page)

between d0_anti-β1 vs. d2_anti-β1, using the d0 states as reference. The top genes from the comparison between d0 and d2 with and without the anti-β1 treatment were visualized using a heatmap (Figure S4). The top DE genes included many known primed markers as well as hESC markers (expressed in primed but also to some extent in naive cells [Sokka et al., 2022]). The effect of anti-β1 treatment was obvious as the degree of capacitation-induced upregulation was clearly more modest in the anti-β1-treated cells when compared to the control cells (Figure S4).

Furthermore, the number of genes significantly upregulated upon capacitation was higher without the anti-β1 treatment (Figure 5G) and included components of the GO term "focal adhesion" (ACTB/HSPA8/PFN1/HSPA5/CALR/PDIA3/HSP90B1/TPM4/RRAS2) (Figure 5H). Interestingly, these included several key regulators of the actin cytoskeleton and cell contractility, concordant with the obvious effect of integrin β1 inhibition attenuating colony morphology changes visible on day 2 of capacitation (Figure 5A). In addition to upregulation of β-actin (ACTB), profilin-1 (PFN1) plays an important role in actin dynamics by regulating actin polymerization in response to extracellular signals (Paavilainen et al., 2004), and tropomyosin-4 (TPM4) upregulation has been shown to correlate with increased actin stress fiber assembly, contractility, and elevation of myosin light-chain phosphorylation (Jiu et al., 2017). Furthermore, calreticulin (CALR) and protein disulfide isomerase Family A Member 3 (PDIA3) are implicated in increased adhesion via supporting maturation and cell surface delivery of glycoproteins, including integrins (Lam and Lim, 2021). Finally, Ras-related protein R-Ras (RRAS) is involved in upregulating integrin activity and trafficking to the membrane (Lilja et al., 2017; Salem et al., 2015). The term "focal adhesion" was also identified in GO analysis of genes downregulated following capacitation but exclusively contained ribosomal proteins. Taken together, these gene expression changes, specifically in the non-integrin-inhibited cells, start to provide insights into the biological players regulating naive stem cell colony morphology. While further studies are needed to fully understand the role of integrin β1 in these cell state transitions, these data are a valuable resource for other researchers in the field interested in the adhesion and biomechanical regulation of stem cells.

DISCUSSION

We describe here unprecedented integrin β1-mediated regulation of human naive and primed PSC states *in vitro*. We demonstrate that integrin β1 is active in naive and primed PSCs when cultured on ECMs commonly used in hiPSC cultures (Matrigel, laminin, and vitronectin) and expressed during early embryo development (laminin). Further, we show that the role of integrin β1 differs in naive and primed states of pluripotency. In primed hiPSCs, active β1 seems to facilitate focal adhesion signaling and mediate forces pulling cells flatter toward ECM. In naive hiPSCs, the amount of active integrin β1 is high but distributes diffusely and fails to activate Src kinase. Furthermore, in naive hiPSCs, integrin β1 does not seem to mediate significant forces pulling colonies flatter toward the ECM. These observations are supported by a recent report detecting increased cell-ECM contractility in mouse ESCs exiting pluripotency (Viswanadha et al., 2024) and human primed PSC nuclei flattening associated with differentiation. Importantly, inhibition of β1 supported naive-like features in primed and naive hiPSCs regarding colony morphology

Figure 5. Integrin β1 inhibition delays the morphological progression of capacitation in naive hiPSCs, giving rise to distinct single-cell transcriptional profiles

(A) Bright-field imaging of naive hiPSCs cultured with anti-β1 (integrin β1 inhibition) or without (non-treated control) at different time points during capacitation (2 or 5 days). Scale bar, 50 μm.

(B) Schematic representation of the experimental setup for the capacitation process and the conditions used for calculating the area ratio shown in (C).

(C) Quantification of colony area ratios (5 independent experiments, t test, p value = 0.0246, mean ± SD). The area ratios are calculated by comparing the colony area of cells after capacitation cultured in NaïveCult to those cultured in E8. These ratios are normalized to the initial area of non-capacitated naive colonies cultured in NaïveCult with or without integrin β1 inhibition.

(D) UMAP of the 6 conditions (naive d0, d2, d0_anti-β1, d2_ anti-β1, primed, and primed_ anti-β1).

(E and F) Visualization and violin blots of the module score expression pattern of naive cell state markers.

(G) Venn diagram showing the number of shared and unique differentially expressed genes between d0 and d2 (naive hiPSC) and d0_anti-β1 and d2_anti-β1 (naive hiPSC + anti-β1) conditions. Up- and downregulated genes are separated by a dashed line and indicated with up or down arrows.

(H) Gene ontology (GO) analysis of differentially expressed genes that were up- or downregulated in control capacitated cells at d2 versus d0 with no change in anti-β1-treated cells. The genes in the "focal adhesion" GO term that were upregulated in control cells following d2 capacitation are listed in the main text. The top 15 Cellular Component GO terms are shown. Count, number of genes per GO term. 81/97 and 62/67 gene names were recognized from up- and downregulated genes in IgG conditions, respectively. Focal adhesion term up in control capacitated cells is highlighted in green. See also Figure S4.

and gene expression patterns. In primed hiPSCs, acute integrin β1 inhibition reduced actomyosin contraction and ERK signaling, whereas continuous integrin inhibition supported maintenance of naive-like state through altered gene expression and attenuated exit from the naive state.

Many protocols for chemical reversion and maintenance of human naive pluripotency *in vitro* have been developed (Hassani et al., 2019; Taei et al., 2020). However, a clear consensus of how different culture methods affect naive hiPSC quality and function is lacking. It was recently reported that integrin β1 inhibition supports the mouse ICM cell organization when cultured in Matrigel (Kim et al., 2022a). This is in line with our results of integrin β1 inhibition supporting naive hiPSC colony compaction when cultured *in vitro*. Together these findings emphasize the importance of integrin-ECM connections in PSC *in vitro* cultures and suggest that integrin β1 inhibition supports the maintenance of early blastocyst ICM cells *in vitro*.

Our transcriptome analysis revealed several interesting candidates linked to β1-integrin regulation of cell states. *AMOTL2* was among the downregulated genes following integrin β1 inhibition in primed hiPSCs. Angiomotin-Like 2 (AMOTL2) interacts with and inhibits transcriptional regulator Yes-associated protein (YAP) in adult cells (Wang et al., 2011; Zhao et al., 2011). In hPSCs, YAP inhibition is needed for actin cytoskeleton reorganization during differentiation into mesodermal cells (Pagliari et al., 2021). Further, AMOTL2 is enriched at the edge of the hPSC colonies where cells are most prone to differentiation *in vitro* (Kim et al., 2022b). The connection of integrin β1 and AMOTL2 in primed hiPSC colony morphology and polarization remains to be studied.

According to our transcriptome analysis, integrin β1 inhibition in naive hiPSCs initiated upregulation of actin regulators, such as Phosphatase Actin Regulator-1 (*PHACTR-1*), which has been previously shown to bind actin and regulate actomyosin assembly and lamellipodium formation (Allain et al., 2012; Jarray et al., 2011; Wiezlak et al., 2012); Smooth Muscle α-actin (*ACTA2*), which regulates vascular contraction and blood pressure (Schildmeyer et al., 2000); and Filamin-A-Binding Protein (*FILIP1*), which regulates cell migration through actin binding protein Filamin-A (Nagano et al., 2002). The role of the aforementioned actin regulators in naive hiPSC maintenance would need further investigation for better understanding of actin regulation in naive pluripotency.

Our capacitation assays further highlight the role of integrin β1 in colony spreading during pluripotency state transitions. Colony spreading due to decreased plasma membrane tension has been linked with naive cells exiting pluripotency in mESCs (De Belly et al., 2021). Our data show that inhibition of integrin β1 has a similar effect to colony morphology as reduced cell surface tension. It is tempting to speculate that activation of cell adhesion receptors would be part of the cascade regulating cell surface mechanics during early differentiation. Integrins are known cellular mechanoregulators, and the functional effect of integrin inhibition is intriguing in light of a recent preprint showing that cell-matrix forces increase during, and are required for, the loss of naive pluripotency in mESCs (Viswanadha et al., 2024). Integrin inhibition most likely counteracts such force buildup providing an interesting mechanistic link to our work. We identified differences in gene expression in naive PSCs capacitated with or without anti-β1-integrin antibodies. Our single-cell analysis revealed that the modular score for naive markers was higher in cells with inhibited integrin β1, which correlates with the observed delay in colony spreading. These findings suggest that integrin β1 inhibition delays the transition from the naive to the primed cell state.

Our study reveals distinct roles of integrin β1 in naive and primed states of pluripotency. In primed pluripotency, active integrin β1 facilitates colony-flattening forces. In contrast, the naive cells show high integrin activity, but this seems interestingly uncoupled from stress fiber contractility, and thus integrin inhibition in these cells has minor morphological influence. Conversely, in naive pluripotency integrin perturbation leads to transcriptional changes undetectable in primed cells. Finally, chemically induced transitions between pluripotency states are linked to upregulation of specific cell adhesion and cytoskeleton contractility regulators, concordant with colony morphology switching.

Taken together, our study reveals that integrin β1 is active in *in vitro*-cultured naive and primed hPSCs, and integrin β1 inhibition induces naive-like characteristics in primed hiPSCs. These data emphasize the importance of the environment and cell-ECM interaction in maintaining the desired cell state in hPSCs and uncover a potentially important functional role for integrin inhibitors in fine-tuning transitions in PSC identity.

METHODS

Reagents

The complete list of antibodies, labels and primers, together with their identifiers, can be found in Table S2.

Cell lines and culture

HiPSC line HEL 24.3 was a kind gift from Timo Otonkoski (the University of Helsinki, Finland) and was generated from human neonatal foreskin fibroblasts by using Sendai viruses (Mikkola et al., 2013; Trokovic et al., 2015). Cells were cultured on Matrigel (354277, Corning)-coated plates in Essential 8 medium (A1517001, Thermo Fisher

Scientific) at +37°C, 5% CO_2. Cells were passaged using a 1:2 to 1:3 split ratio every 3–4 days or once 80% confluency was reached. 50 mM EDTA in phosphate-buffered saline (PBS) was used for cell dissociation (Närvä et al., 2017), and Essential 8 medium was changed daily.

AICS-0016 (WTC-mEGFP-ACTB-cl184, RRID: CVCL_JM16) hiPSCs were cultured on Matrigel (354230, Corning)-coated plates in mTeSR1 (85850, STEMCELL Technologies) medium at +37°C, 5% CO_2. 50 mM EDTA in PBS was used for passaging of the cells (Närvä et al., 2017), and culture medium was changed daily.

PSC cryopreservation medium (Gibco) was used when freezing the hiPSCs, and RevitaCell supplement (A2644501, Gibco) was added in the culture medium when reviving the cells.

Naive-like hESCs were a kind gift from Timo Otonkoski (the University of Helsinki, Finland).

Mouse (ICR)-inactivated embryonic fibroblasts (commercial iMEFs, A24903, Life Technologies) were cultured in DMEM/F12 (11320033, Gibco) supplemented with 10% FBS (Sigma-Aldrich) at +37°C, 5% CO_2 and washed twice with PBS before using as feeder cells for naive hiPSCs.

The generation of *cpdm* mouse embryonic fibroblasts (MEFs) has been described before (Rantala et al., 2011). The MEFs were cultured in Dulbecco's modified Eagle's medium (DMEM, Sigma-Aldrich) supplemented with 10% fetal bovine serum (FBS, Sigma-Aldrich), 2 mM L-glutamine (Sigma-Aldrich), 1% sodium pyruvate (Sigma-Aldrich), 1% non-essential amino acid solution (Sigma-Aldrich), 1% penicillin-streptomycin (Sigma-Aldrich), and 0.001% beta-mercaptoethanol (M3148, Sigma-Aldrich) at +37°C, 5% CO_2. Prior to using as feeder cells (in-house iMEFs), the MEFs were plated on 0.1% gelatin (07903, STEMCELL Technologies)-coated plates, and, after reaching full confluency, the proliferation of the MEFs was stopped by treating the cells with Mitomycin C (M4287, Sigma) for 3 h at 37°C, followed by a PBS wash.

All cell lines were tested and confirmed negative for mycoplasma contamination regularly. We used the lowest possible passage number, not exceeding 49 with the primed hiPSCs and 22 with the naive hiPSCs.

Reversion to naive-like state

HEL 24.3 hiPS cells were plated on an iMEF monolayer and reverted into a naive-like state by using NaïveCult induction kit (05580, STEMCELL Technologies) according to manufacturer's instructions. In order to inhibit integrin β1 activity, 5 μg/mL rat anti-human β1-integrin antibody (mAb13) was included in the culture medium throughout and after the reversion, except during re-plating of the cells. Cells were detached by using StemPro Accutase cell dissociation reagent (A1110501, Gibco) and replated in culture medium supplemented with 10 μM ROCK inhibitor Y-27632 (72302, STEMCELL Technologies).

Maintenance of naive hiPSC

After reversion, the naive hiPSCs were cultured on commercial or in-house iMEFs in NaïveCult expansion medium (05590, STEMCELL Technologies) or in-house tt2iLGö medium: N2B27 (DMEM/F12 [1:2; 11320033, Gibco], Neurobasal medium [1:2; 21103049, Gibco], N2 supplement [in-house], 1 mM L-glutamine [Sigma-Aldrich], and 0.1 mM β-mercaptoethanol [M3148, Sigma-Aldrich]) medium supplemented with 0.3 μM CHIR99021 (SML1046, Sigma-Aldrich), 1 μM PDO325901 (PZ0162, Sigma-Aldrich), 10 ng/mL human leukemia inhibitory factor (LIF, 78055.1, STEMCELL Technologies), and 2 μM Gö6983 (2285, Tocris Bioscience) at +37°C, 5% O_2, 5% CO_2 (Guo et al., 2017). N2 was prepared by supplementing DMEM/F12 with 0.4 mg/mL insulin (I9278, Sigma-Aldrich), 10 mg/mL apo-transferrin (3188-AT-001G, R&D Systems), 3 μM sodium selenite (S5261, Sigma-Aldrich), 1.6 mg/mL putrescine (P5780-5G, Sigma-Alrich), and 2 μg/mL progesterone (P8783, Sigma-Aldrich). Culture medium was changed daily, and cells were passaged every 3–4 days with a 1:2 to 1:5 ratio. Cells were detached by using StemPro Accutase cell dissociation reagent (A1110501, Gibco) or TrypLE Express (12604-21, Gibco) and replated in culture medium supplemented with 10 μM ROCK inhibitor Y-27632 (72302, STEMCELL Technologies). PSC cryopreservation medium (Gibco) was used for freezing of the naive hiPSCs, and 10 μM ROCK inhibitor Y-27632 (72302, STEMCELL Technologies) was added in the culture medium when reviving the cells.

Immunofluorescence

μ-slide 8 well (ibidi) chambered coverslips were coated with Matrigel (354277, Corning), 5 μg/mL vitronectin (A14700, Gibco), or 5 μg/mL laminin-521 (A29248, Gibco) at 37°C for 1 h. Cells were plated on coated μ-slide wells and were grown and treated with antibodies until the time points indicated in the figure legends and main text. Culture medium was changed daily from the cells that were grown more than 24 h. Cells were fixed with 4% PFA, washed with PBS, incubated with 0.1 M glycine for 10 min at room temperature (RT), washed with PBS, permeabilized with 0.3% Triton X-100 for 10 min at RT, washed again with PBS, and incubated with primary antibodies in 1% BSA in PBS overnight at 4°C. Cells were washed with PBS and PBST (0.05% Tween in PBS), and incubated with secondary antibodies, 4′,6-diamidino-2-phenylindole (DAPI), dihydrochloride, SiR-Actin (0.5 μM), or Atto-Phalloidin for 1 h at RT. Cells were washed with PBS prior to imaging.

Confocal microscopy, live-cell imaging, and image analysis

Immunofluorescence-stained cells were imaged using 3i CSU-W1 spinning disk confocal microscope, sCMOS Orca Flash4.0×(Hamamatsu) camera, and 63× Plan-Apochromat (Zeiss) objective (Figures 1C, 1E, 1G, S1H, 2D, 2E, S2C–S2E, 3A, S3C, S3D, 4C, and 4D). Live-cell imaging was performed using IncyCyte S3 live-cell analysis instrument (Satorius), 10x objective, and phase contrast channel (Figures 1A, 2B, and 5A and Videos S1 and S2). Bright-field images were taken using EVOS FL fluorescence microscope (Figures S1B and 4B). All of the images were analyzed using ImageJ.

Western Blot

Cells were grown and treated with antibodies until the time points indicated in the figure legends and main text, washed with PBS on ice, lysed using Triton X-100 lysis buffer (TXLB; 50 mM Tris-HCl, pH 7.5, 150 mM NaCl, 0.5% Triton X-100, 0.5% glycerol, 1% SDS, cOmplete protease inhibitor [Sigma-Aldrich], and PhosSTOP tablet [Sigma-Aldrich]), and collected by scraping. Samples were boiled for 5 min and sonicated. Protein concentrations were measured using DC Protein assay (Bio-Rad) and normalized by adding TXLB. SDS sample buffer was added on the samples, and the samples were boiled for 5 min and loaded on precast Tris-Glycine-eXtendet SDS-PAGE gels with a 4%–20% gradient (Bio-Rad). After separation, the proteins were transferred on nitrocellulose membranes (Bio-Rad) using the Trans-Blot Turbo Transfer System (Bio-Rad), followed by blocking with 5% milk powder in Tris-buffered saline (TBS) with 0.1% Tween 20 (TBST) for 1 h at RT. Membranes were incubated with primary antibodies diluted in AdvanBlock-Fluor blocking solution (Advansta) overnight at +4°C, washed three times with TBST, and incubated with fluorophore-conjugated Odyssey or Azure secondary antibodies (LI-COR Biosciences) for 1 h at RT. Membranes were washed three times with TBST and scanned with Odyssey infrared system (LI-COR Biosciences) or Sapphire Biomolecular RGBNIR Imager (Azure). Protein band intensities were analyzed using ImageJ.

qPCR

Total RNA was extracted using the NucleoSpin RNA kit (#740955.250, Macherey-Nagel) according to manufacturers' instructions from cells that were grown and treated with antibodies until the time points indicated in the figure legends and main text. Complementary DNA synthesis from RNA was performed using high-capacity cDNA reverse-transcription kit (Thermo Fisher Scientific). The expression levels of target genes were determined with QuantStudio 12K Flex real-time PCR system (Thermo Fisher Scientific).

Capacitation

For the capacitation process, naive hiPSCs were first plated on Matrigel-precoated plates (354277, Corning) supplemented with 10 μM Y-27632 (72302, STEMCELL Technologies). After two days, the NaïveCult medium was changed to capacitation medium, called N2B27, as described in Rostovskaya et al. (2019) (DMEM/F12 [1:2; 11320033, Gibco], Neurobasal medium [1:2; 21103049, Gibco], N2 supplement [in-house], 1 mM L-glutamine [Sigma-Aldrich], and 0.1 mM β-mercaptoethanol [M3148, Sigma-Aldrich]) supplemented with 2 μM XAV-939 (Tocris Bio-Techne, 3748) at +37°C, 5% CO_2 (Guo et al., 2017). N2 was prepared by supplementing DMEM/F12 with 0.4 mg/mL insulin (I9278, Sigma-Aldrich), 10 mg/mL apo-transferrin (3188-AT-001G, R&D Systems), 3 μM sodium selenite (S5261, Sigma-Aldrich), 1.6 mg/mL putrescine (P5780-5G, Sigma-Alrich), and 2 μg/mL progesterone (P8783, Sigma-Aldrich). Depending on the experiment, the cells were capacitated for 2 to 5 days. The capacitation process was followed with an Incucyte S3 live-cell analysis instrument (Sartorius).

RNA sequencing

RNA was isolated from three biological replicates of IgG- or MAb13-treated (12 h) primed hiPSCs, naive hiPSCs, and naive + MAb13 hiPSCs, using NucleoSpin RNA kit (#740955.250, Macherey-Nagel). The quality of the samples was verified using Agilent Bioanalyzer 2100, and the sample concentrations were measured using Qubit/Quant-iT fluorometric quantitation (Life Technologies). For the library preparation, 100 ng of RNA was amplified by using Illumina stranded mRNA preparation, ligation kit (Illumina) according to manufacturer's protocol. The quality of the library was verified using Advanced Analytical Fragment Analyzer, and sample concentrations were measured using Qubit/Quant-iT fluorometric quantitation (Life Technologies). Sequencing was performed using NovaSeq 6000 S4 instrument, v.1.5 (Illumina).

The sequencing data read quality was ensured using the FastQ (v.0.11.14, http://www.bioinformatics.babraham.ac.uk/projects/fastqc) and MultiQC (v.1.5) (Ewels et al., 2016) tools. Differentially expressed genes were identified between the IgG- or MAb13-treated primed hiPSCs and between the naive hiPSCs and naive + MAb13 hiPSCs. DE analysis was performed using Bioconductor R package ROTS (v.1.14.0) (Suomi et al., 2017). Genes with FDR <0.05 were defined as differentially expressed. Gene-annotation enrichment analysis of differentially expressed genes was done by using The Database for Annotation, Visualization and Integrated Discovery (DAVID) annotation tools (Huang et al., 2009a, 2009b).

scRNA-seq

scRNA-seq libraries were prepared using 10× Genomics Chromium Next GEM Single Cell 3' Reagent Kits v3.1 (Dual Index), following manufacturer's instructions (Protocol number CG000315). In brief, cells were treated with reagents and antibodies until the time points indicated in the main text and figure legends, and from each sample 3,000–15,000 cells were loaded on Chromium Next GEM Chip G and partitioned into droplets using a Chromium X instrument (10× Genomics). The PCR steps were performed with a C1000 Touch Thermal Cycler with 96-Deep Well Reaction Module (Bio-Rad), using 13 cycles for the cDNA amplification and either 12 or 14 cycles for the sample index PCR. The libraries were sequenced using an Illumina NovaSeq 6000 instrument and an S2 flow cell with the following read length configuration: Read1 = 28, i7 = 10, i5 = 10, Read2 = 90.

Quality control and workflow before downstream analyses

The single-cell data analyses were run in R (v.4.2.1) (R Core Team, 2021). All the analyses were performed using the Finnish CSC IT Center for Science web interface of the Puhti supercomputer. The first step was quality control, which included pre-processing of the data using Seurat v.4.1.1. Each sample was quality controlled individually (Hao et al., 2021). During this step we did a crude pruning of the low-quality cells. First, by using filtering thresholds on the number of features where the lower cutoff was 500 and the upper limit was 5,000 (the upper limit varied between samples and was evaluated visually from violin plots). The mitochondrial content threshold varied between 5% and 10% depending on the sample. After the crude filtering of the samples, we normalized (LogNormalization) and scaled the data using Seurat. This was required as an initial step for the removal of cell doublets with DoubletFinder (v.2.0.3) (McGinnis et al., 2019). For the DoubletFinder we used the expected multiplet rate depending on number of cells loaded from the 10× Genomics CG000315 Rev A manual. For our samples, this varied between 0.005 and 0.096 (or 0.5%–9.6%). We expected quite a few doublets based on the loading numbers of the samples. However, after the crude pruning and subsequent doublet removal, we were confident that the resulting data did not have a significant number of doublets remaining.

Next, we merged all the samples into one large Seurat object. We used the "vst" method for finding the variable features using a threshold to return 3,000 features. Rescaling of the data and running principal-component analysis (PCA) for dimensional reduction was performed using default parameters. Based on an elbow plot, first six principal components were selected. Using this PCA with 1:6 dimensions, we ran UMAP, computed k-nearest neighbors, and carried out unsupervised clustering. Appropriate clustering resolution was checked using Clustree package (v.0.5.5) (Zappia and Oshlack, 2018) ranging from 0 to 1 by intervals of 0.1. We determined that a suitable clustering resolution for our dataset was 0.2.

Downstream analyses of the scRNA-seq data

Differentially expressed gene analysis was carried out in Seurat using the Wilcoxon rank-sum test. We first merged the naive cells without anti-β1 (d0 and d2) as one object and with anti-β1 (d0_anti β1 and d2_anti β1) as another object. Both datasets were rescaled and reclustered with resolution 0.2 before analysis. In the analysis, we set d0 as the reference (ident = 2) and d2 as the "case" (ident = 1).

The comparison of differentially expressed gene lists was performed using VennDiagram package (v.1.7.3) (Chen and Boutros, 2011). For upregulated genes, we filtered the lists using p_val_adj < 0.05 & avg_log2FC > 0.5 and for downregulated genes we used p_val_adj < 0.05 & avg_log2FC < −0.5. We were also interested in the genes that were differentially expressed between d0 vs. d2 but were not differentially expressed between d0_anti-β1 vs. d2_anti-β1. For d0 vs. d2, filtering was done using (p_val_adj < 0.05 & avg_log2FC > −0.5 & avg_log2FC < 0.5) whereas filtering for d0_ anti-β1 vs. d2_ anti-β1 was done using p_val_adj < 0.05 & avg_log2FC < −0.5 | avg_log2FC > 0.5. GO was performed with clusterProfiler (version 4.8.3 [Wu et al., 2021]) in R.

Module scores were calculated in Seurat using the AddModuleScore function, which calculates the average expression levels of genes of interest in relation to a randomly selected reference gene set. For this function, we set the number of control genes to 5 and number of bins to 10. The genes considered as naive markers were: *CHODL*, *NLRP7*, *SLC16A10*, *UTF1*, *MT1G*, *AC011447.3*, *ZYG11A*, *CBFA2T2*, *MT1H*, *ZNF600*, *AKAP12*, *TRIML2*, *WDHD1*, *PRODH*, *RESF1*, *SERPINB9*, *NLRP2*, *NLRP1*, *ASRGL1*, *AC092546.1*, *LINC01950*, *PTCHD1*, *SLC25A16*, *DNMT3L*, *ZNF729*, *CNR2*, *PBX4*, and *BRDT*.

RESOURCE AVAILABILITY

Lead contact

Further inquiries should be directed to the lead contact, Johanna Ivaska (Johanna.ivaska@utu.fi).

Materials availability

This study did not generate unique reagents.

Data and code availability

The RNA sequencing data have been deposited at Gene Expression Omnibus (GEO) and are publicly available as of the date of

publication (GEO accession numbers: GSE205423 and GSE282224). All other data supporting the findings of this study are available within the paper and its supplementary information files.

ACKNOWLEDGMENTS

We thank J. Siivonen and P. Laasola for technical assistance. The Ivaska laboratory is acknowledged for lively discussions and critical feedback on the manuscript and H. Hamidi for editing the manuscript. We thank Prof. T. Otonkoski for providing cell lines. The Cell Imaging and Cytometry core facility (Turku Bioscience Centre, University of Turku; Åbo Akademi University; and Biocenter Finland), the Euro-Bioimaging node in Turku, the Finnish Functional Genomics Centre, and the single-cell omics core facility (Turku Bioscience Centre, University of Turku, and Åbo Akademi University) are acknowledged for services, instrumentation, and expertise. We thank the Medical Bioinformatics Centre of Turku Bioscience Centre for the sequencing data analysis. The Centre is supported by the University of Turku, Åbo Akademi University, Biocenter Finland, and ELIXIR Finland. We acknowledge CSC – IT Center for Science, Finland, for providing computational resources. This study was supported by the Research Council of Finland (J.I. 330033; 325464), Research Council of Finland CoE in Cell and Tissue Mechanics (J.I. 364182), InFLAMES Flagship Programme of the Research Council of Finland (decision number: 337530), the Sigrid Juselius Foundation (J.I.), and European Research Council Advanced Grant (101142305). M.E.T. has been supported by the University of Turku Doctoral Program for Molecular Medicine, Finnish Cultural Foundation, K. Albin Johansson Foundation, and Magnus Ehrnrooth Foundation. N.P. has been supported by the "PhD in Oncology" program from the Philantropia Foundation and the Turku University Foundation. S.J. has been supported by the Turku University Foundation. J.S. and R.T. have been supported by the Jane and Aatos Erkko Foundation.

AUTHOR CONTRIBUTIONS

Conceptualization, M.E.T., L.M., and J.I.; investigation, M.E.T., N. P., A.S., P.R., S.V., M.R.C., and J.S.; formal analysis, M.E.T., N.P., S.J., L.M., and M.R.C.; writing – original draft, M.E.T. and J.I.; writing – editing, M.E.T., N.P., A.S., R.T., L.M., S.J., T.L., and J.I.; visualization, M.E.T., N.P., S.J., L.M., and M.R.C.; supervision, J.I., L.M., R.T., and T.L.; funding acquisition, J.I.

DECLARATION OF INTERESTS

The authors declare no competing interests.

SUPPLEMENTAL INFORMATION

Supplemental information can be found online at https://doi.org/10.1016/j.stemcr.2025.102538.

Received: October 23, 2024
Revised: May 21, 2025
Accepted: May 22, 2025
Published: June 19, 2025

REFERENCES

Allain, B., Jarray, R., Borriello, L., Leforban, B., Dufour, S., Liu, W.q., Pamonsinlapatham, P., Bianco, S., Larghero, J., Hadj-Slimane, R., et al. (2012). Neuropilin-1 regulates a new VEGF-induced gene, Phactr-1, which controls tubulogenesis and modulates lamellipodial dynamics in human endothelial cells. Cell. Signal. *24*, 214–223. https://doi.org/10.1016/j.cellsig.2011.09.003.

Brakebusch, C., and Fässler, R. (2003). The integrin-actin connection, an eternal love affair. EMBO J. *22*, 2324–2333. https://doi.org/10.1093/emboj/cdg245.

Bredenkamp, N., Yang, J., Clarke, J., Stirparo, G.G., von Meyenn, F., Dietmann, S., Baker, D., Drummond, R., Ren, Y., Li, D., et al. (2019). Wnt Inhibition Facilitates RNA-Mediated Reprogramming of Human Somatic Cells to Naive Pluripotency. Stem Cell Rep. *13*, 1083–1098. https://doi.org/10.1016/j.stemcr.2019.10.009.

Byron, A., Humphries, J.D., Askari, J.A., Craig, S.E., Mould, A.P., and Humphries, M.J. (2009). Anti-integrin monoclonal antibodies. J. Cell Sci. *122*, 4009–4011. https://doi.org/10.1242/jcs.056770.

Campbell, I.D., and Humphries, M.J. (2011). Integrin Structure, Activation, and Interactions. Cold Spring Harb. Perspect. Biol. *3*, a004994. https://doi.org/10.1101/cshperspect.a004994.

Chen, H., and Boutros, P.C. (2011). VennDiagram: a package for the generation of highly-customizable Venn and Euler diagrams in R. BMC Bioinf. *12*, 35. https://doi.org/10.1186/1471-2105-12-35.

Collier, A.J., Bendall, A., Fabian, C., Malcolm, A.A., Tilgner, K., Semprich, C.I., Wojdyla, K., Nisi, P.S., Kishore, K., Roamio Franklin, V.N., et al. (2022). Genome-wide screening identifies Polycomb repressive complex 1.3 as an essential regulator of human naïve pluripotent cell reprogramming. Sci. Adv. *8*, eabk0013. https://doi.org/10.1126/sciadv.abk0013.

De Belly, H., Stubb, A., Yanagida, A., Labouesse, C., Jones, P.H., Paluch, E.K., and Chalut, K.J. (2021). Membrane Tension Gates ERK-Mediated Regulation of Pluripotent Cell Fate. Cell Stem Cell *28*, 273–284.e6. https://doi.org/10.1016/j.stem.2020.10.018.

Ding, T., Zhou, Y., Long, R., Chen, C., Zhao, J., Cui, P., Guo, M., Liang, G., and Xu, L. (2019). DUSP8 phosphatase: structure, functions, expression regulation and the role in human diseases. Cell Biosci. *9*, 70. https://doi.org/10.1186/s13578-019-0329-4.

Fässler, R., Pfaff, M., Murphy, J., Noegel, A.A., Johansson, S., Timpl, R., and Albrecht, R. (1995). Lack of beta 1 integrin gene in embryonic stem cells affects morphology, adhesion, and migration but not integration into the inner cell mass of blastocysts. J. Cell Biol. *128*, 979–988. https://doi.org/10.1083/jcb.128.5.979.

Guo, G., von Meyenn, F., Rostovskaya, M., Clarke, J., Dietmann, S., Baker, D., Sahakyan, A., Myers, S., Bertone, P., Reik, W., et al. (2017). Epigenetic resetting of human pluripotency. Development *144*, 2748–2763. https://doi.org/10.1242/dev.146811.

Hao, Y., Hao, S., Andersen-Nissen, E., Mauck, W.M., 3rd, Zheng, S., Butler, A., Lee, M.J., Wilk, A.J., Darby, C., Zager, M., et al. (2021). Integrated analysis of multimodal single-cell data. Cell *184*, 3573–3587.e29. https://doi.org/10.1016/j.cell.2021.04.048.

Hassani, S.-N., Moradi, S., Taleahmad, S., Braun, T., and Baharvand, H. (2019). Transition of inner cell mass to embryonic stem

cells: mechanisms, facts, and hypotheses. Cell. Mol. Life Sci. *76*, 873–892. https://doi.org/10.1007/s00018-018-2965-y.

Huang, D.W., Sherman, B.T., and Lempicki, R.A. (2009a). Systematic and integrative analysis of large gene lists using DAVID bioinformatics resources. Nat. Protoc. *4*, 44–57. https://doi.org/10.1038/nprot.2008.211.

Huang, D.W., Sherman, B.T., Zheng, X., Yang, J., Imamichi, T., Stephens, R., and Lempicki, R.A. (2009b). Extracting Biological Meaning from Large Gene Lists with DAVID. Curr. Protoc. Bioinformatics *Chapter 13*. Unit 13.11.1-13.11.13. https://doi.org/10.1002/0471250953.bi1311s27.

Hynes, R.O. (2002). Integrins: bidirectional, allosteric signaling machines. Cell *110*, 673–687. https://doi.org/10.1016/s0092-8674(02)00971-6.

Jarray, R., Allain, B., Borriello, L., Biard, D., Loukaci, A., Larghero, J., Hadj-Slimane, R., Garbay, C., Lepelletier, Y., and Raynaud, F. (2011). Depletion of the novel protein PHACTR-1 from human endothelial cells abolishes tube formation and induces cell death receptor apoptosis. Biochimie *93*, 1668–1675. https://doi.org/10.1016/j.biochi.2011.07.010.

Jiu, Y., Peränen, J., Schaible, N., Cheng, F., Eriksson, J.E., Krishnan, R., and Lappalainen, P. (2017). Vimentin intermediate filaments control actin stress fiber assembly through GEF-H1 and RhoA. J. Cell Sci. *130*, 892–902. https://doi.org/10.1242/jcs.196881.

Kim, E.J.Y., Sorokin, L., and Hiiragi, T. (2022a). ECM-integrin signalling instructs cellular position sensing to pattern the early mouse embryo. Development *149*, dev200140. https://doi.org/10.1242/dev.200140.

Kim, Y., Jang, H., Seo, K., Kim, J.H., Lee, B., Cho, H.M., Kim, H.J., Yang, E., Kim, H., Gim, J.A., et al. (2022b). Cell position within human pluripotent stem cell colonies determines apical specialization via an actin cytoskeleton-based mechanism. Stem Cell Rep. *17*, 68–81. https://doi.org/10.1016/j.stemcr.2021.11.005.

Lam, S.T.T., and Lim, C.J. (2021). Cancer Biology of the Endoplasmic Reticulum Lectin Chaperones Calreticulin, Calnexin and PDIA3/ERp57. Prog. Mol. Subcell. Biol. *59*, 181–196. https://doi.org/10.1007/978-3-030-67696-4_9.

Lilja, J., Zacharchenko, T., Georgiadou, M., Jacquemet, G., De Franceschi, N., Peuhu, E., Hamidi, H., Pouwels, J., Martens, V., Nia, F.H., et al. (2017). SHANK proteins limit integrin activation by directly interacting with Rap1 and R-Ras. Nat. Cell Biol. *19*, 292–305. https://doi.org/10.1038/ncb3487.

Lynch, C.J., Bernad, R., Martínez-Val, A., Shahbazi, M.N., Nóbrega-Pereira, S., Calvo, I., Blanco-Aparicio, C., Tarantino, C., Garreta, E., Richart-Ginés, L., et al. (2020). Global hyperactivation of enhancers stabilizes human and mouse naive pluripotency through inhibition of CDK8/19 Mediator kinases. Nat. Cell Biol. *22*, 1223–1238. https://doi.org/10.1038/s41556-020-0573-1.

Martinez-Val, A., Lynch, C.J., Calvo, I., Ximénez-Embún, P., Garcia, F., Zarzuela, E., Serrano, M., and Munoz, J. (2021). Dissection of two routes to naïve pluripotency using different kinase inhibitors. Nat. Commun. *12*, 1863. https://doi.org/10.1038/s41467-021-22181-5.

McGinnis, C.S., Murrow, L.M., and Gartner, Z.J. (2019). DoubletFinder: Doublet Detection in Single-Cell RNA Sequencing Data Using Artificial Nearest Neighbors. Cell Syst. *8*, 329–337.e4. https://doi.org/10.1016/j.cels.2019.03.003.

Mikkola, M., Toivonen, S., Tamminen, K., Alfthan, K., Tuuri, T., Satomaa, T., Natunen, J., Saarinen, J., Tiittanen, M., Lampinen, M., et al. (2013). Lectin from Erythrina cristagalli supports undifferentiated growth and differentiation of human pluripotent stem cells. Stem Cells Dev. *22*, 707–716. https://doi.org/10.1089/scd.2012.0365.

Molè, M.A., Weberling, A., Fässler, R., Campbell, A., Fishel, S., and Zernicka-Goetz, M. (2021). Integrin β1 coordinates survival and morphogenesis of the embryonic lineage upon implantation and pluripotency transition. Cell Rep. *34*, 108834. https://doi.org/10.1016/j.celrep.2021.108834.

Nagano, T., Yoneda, T., Hatanaka, Y., Kubota, C., Murakami, F., and Sato, M. (2002). Filamin A-interacting protein (FILIP) regulates cortical cell migration out of the ventricular zone. Nat. Cell Biol. *4*, 495–501. https://doi.org/10.1038/ncb808.

Närvä, E., Stubb, A., Guzmán, C., Blomqvist, M., Balboa, D., Lerche, M., Saari, M., Otonkoski, T., and Ivaska, J. (2017). A Strong Contractile Actin Fence and Large Adhesions Direct Human Pluripotent Colony Morphology and Adhesion. Stem Cell Rep. *9*, 67–76. https://doi.org/10.1016/j.stemcr.2017.05.021.

Nichols, J., and Smith, A. (2009). Naive and primed pluripotent states. Cell Stem Cell *4*, 487–492. https://doi.org/10.1016/j.stem.2009.05.015.

Nichols, J., Silva, J., Roode, M., and Smith, A. (2009). Suppression of Erk signalling promotes ground state pluripotency in the mouse embryo. Development *136*, 3215–3222. https://doi.org/10.1242/dev.038893.

Paavilainen, V.O., Bertling, E., Falck, S., and Lappalainen, P. (2004). Regulation of cytoskeletal dynamics by actin-monomer-binding proteins. Trends Cell Biol. *14*, 386–394. https://doi.org/10.1016/j.tcb.2004.05.002.

Pagliari, S., Vinarsky, V., Martino, F., Perestrelo, A.R., Oliver De La Cruz, J., Caluori, G., Vrbsky, J., Mozetic, P., Pompeiano, A., Zancla, A., et al. (2021). YAP-TEAD1 control of cytoskeleton dynamics and intracellular tension guides human pluripotent stem cell mesoderm specification. Cell Death Differ. *28*, 1193–1207. https://doi.org/10.1038/s41418-020-00643-5.

Pera, M.F., and Rossant, J. (2021). The exploration of pluripotency space: Charting cell state transitions in peri-implantation development. Cell Stem Cell *28*, 1896–1906. https://doi.org/10.1016/j.stem.2021.10.001.

R Core Team (2021). R: A Language and Environment for Statistical Computing.

Rantala, J.K., Pouwels, J., Pellinen, T., Veltel, S., Laasola, P., Mattila, E., Potter, C.S., Duffy, T., Sundberg, J.P., Kallioniemi, O., et al. (2011). SHARPIN is an endogenous inhibitor of β1-integrin activation. Nat. Cell Biol. *13*, 1315–1324. https://doi.org/10.1038/ncb2340.

Rostovskaya, M., Stirparo, G.G., and Smith, A. (2019). Capacitation of human naïve pluripotent stem cells for multi-lineage differentiation. Development *146*, dev172916. https://doi.org/10.1242/dev.172916.

Salem, J.C., Reviriego-Mendoza, M.M., and Santy, L.C. (2015). ARF-GEF cytohesin-2/ARNO regulates R-Ras and α5-integrin recycling through an EHD1-positive compartment. Mol. Biol. Cell *26*, 4265–4279. https://doi.org/10.1091/mbc.E15-05-0278.

Schildmeyer, L.A., Braun, R., Taffet, G., Debiasi, M., Burns, A.E., Bradley, A., and Schwartz, R.J. (2000). Impaired vascular contractility and blood pressure homeostasis in the smooth muscle alpha-actin null mouse. FASEB J. *14*, 2213–2220. https://doi.org/10.1096/fj.99-0927com.

Sim, Y.-J., Kim, M.S., Nayfeh, A., Yun, Y.J., Kim, S.J., Park, K.T., Kim, C.H., and Kim, K.S. (2017). 2i Maintains a Naive Ground State in ESCs through Two Distinct Epigenetic Mechanisms. Stem Cell Rep. *8*, 1312–1328. https://doi.org/10.1016/j.stemcr.2017.04.001.

Sokka, J., Yoshihara, M., Kvist, J., Laiho, L., Warren, A., Stadelmann, C., Jouhilahti, E.M., Kilpinen, H., Balboa, D., Katayama, S., et al. (2022). CRISPR activation enables high-fidelity reprogramming into human pluripotent stem cells. Stem Cell Rep. *17*, 413–426. https://doi.org/10.1016/j.stemcr.2021.12.017.

Stephens, L.E., Sutherland, A.E., Klimanskaya, I.V., Andrieux, A., Meneses, J., Pedersen, R.A., and Damsky, C.H. (1995). Deletion of beta 1 integrins in mice results in inner cell mass failure and peri-implantation lethality. Genes Dev. *9*, 1883–1895. https://doi.org/10.1101/gad.9.15.1883.

Stubb, A., Guzmán, C., Närvä, E., Aaron, J., Chew, T.L., Saari, M., Miihkinen, M., Jacquemet, G., and Ivaska, J. (2019). Superresolution architecture of cornerstone focal adhesions in human pluripotent stem cells. Nat. Commun. *10*, 4756. https://doi.org/10.1038/s41467-019-12611-w.

Suomi, T., Seyednasrollah, F., Jaakkola, M.K., Faux, T., and Elo, L.L. (2017). ROTS: An R package for reproducibility-optimized statistical testing. PLoS Comput. Biol. *13*, e1005562. https://doi.org/10.1371/journal.pcbi.1005562.

Taei, A., Rasooli, P., Braun, T., Hassani, S.N., and Baharvand, H. (2020). Signal regulators of human naïve pluripotency. Exp. Cell Res. *389*, 111924. https://doi.org/10.1016/j.yexcr.2020.111924.

Takahashi, K., and Yamanaka, S. (2006). Induction of pluripotent stem cells from mouse embryonic and adult fibroblast cultures by defined factors. Cell *126*, 663–676. https://doi.org/10.1016/j.cell.2006.07.024.

Takahashi, K., Tanabe, K., Ohnuki, M., Narita, M., Ichisaka, T., Tomoda, K., and Yamanaka, S. (2007). Induction of pluripotent stem cells from adult human fibroblasts by defined factors. Cell *131*, 861–872. https://doi.org/10.1016/j.cell.2007.11.019.

Takashima, Y., Guo, G., Loos, R., Nichols, J., Ficz, G., Krueger, F., Oxley, D., Santos, F., Clarke, J., Mansfield, W., et al. (2014). Resetting transcription factor control circuitry toward ground-state pluripotency in human. Cell *158*, 1254–1269. https://doi.org/10.1016/j.cell.2014.08.029.

Theunissen, T.W., Powell, B.E., Wang, H., Mitalipova, M., Faddah, D.A., Reddy, J., Fan, Z.P., Maetzel, D., Ganz, K., Shi, L., et al. (2014). Systematic identification of culture conditions for induction and maintenance of naive human pluripotency. Cell Stem Cell *15*, 471–487. https://doi.org/10.1016/j.stem.2014.07.002.

Trokovic, R., Weltner, J., and Otonkoski, T. (2015). Generation of iPSC line HEL24.3 from human neonatal foreskin fibroblasts. Stem Cell Res. *15*, 266–268. https://doi.org/10.1016/j.scr.2015.05.012.

Viswanadha, S., Gómez-González, M., Labouesse, C., Venturini, V., Trepat, X., Chalut, K., Kechagia, Z., and Roca-Cusachs, P. (2024). Cell-matrix force transmission regulates the loss of naïve pluripotency in mouse embryonic stem cells. Preprint at bioRxiv. https://doi.org/10.1101/2024.05.13.593501.

Wang, W., Huang, J., and Chen, J. (2011). Angiomotin-like proteins associate with and negatively regulate YAP1. J. Biol. Chem. *286*, 4364–4370. https://doi.org/10.1074/jbc.C110.205401.

Weinberger, L., Ayyash, M., Novershtern, N., and Hanna, J.H. (2016). Dynamic stem cell states: naive to primed pluripotency in rodents and humans. Nat. Rev. Mol. Cell Biol. *17*, 155–169. https://doi.org/10.1038/nrm.2015.28.

Wiezlak, M., Diring, J., Abella, J., Mouilleron, S., Way, M., McDonald, N.Q., and Treisman, R. (2012). G-actin regulates the shuttling and PP1 binding of the RPEL protein Phactr1 to control actomyosin assembly. J. Cell Sci. *125*, 5860–5872. https://doi.org/10.1242/jcs.112078.

Wojdyla, K., Collier, A.J., Fabian, C., Nisi, P.S., Biggins, L., Oxley, D., and Rugg-Gunn, P.J. (2020). Cell-Surface Proteomics Identifies Differences in Signaling and Adhesion Protein Expression between Naive and Primed Human Pluripotent Stem Cells. Stem Cell Rep. *14*, 972–988. https://doi.org/10.1016/j.stemcr.2020.03.017.

Wu, T., Hu, E., Xu, S., Chen, M., Guo, P., Dai, Z., Feng, T., Zhou, L., Tang, W., Zhan, L., et al. (2021). clusterProfiler 4.0: A universal enrichment tool for interpreting omics data. Innovation *2*, 100141. https://doi.org/10.1016/j.xinn.2021.100141.

Zappia, L., and Oshlack, A. (2018). Clustering trees: a visualization for evaluating clusterings at multiple resolutions. GigaScience *7*, giy083. https://doi.org/10.1093/gigascience/giy083.

Zhao, B., Li, L., Lu, Q., Wang, L.H., Liu, C.Y., Lei, Q., and Guan, K.L. (2011). Angiomotin is a novel Hippo pathway component that inhibits YAP oncoprotein. Genes Dev. *25*, 51–63. https://doi.org/10.1101/gad.2000111.